This information is current as of October 12, 2024.

# Fat-suppression failure artifacts simulating pathology on frequency-selective fat-suppression MR images of the head and neck.

Y Anzai, R B Lufkin, B A Jabour and W N Hanafee

*AJNR Am J Neuroradiol* 1992, 13 (3) 879-884
http://www.ajnr.org/content/13/3/879

# Fat-Suppression Failure Artifacts Simulating Pathology on Frequency-Selective Fat-Suppression MR Images of the Head and Neck

Yoshimi Anzai,[1,2] Robert B. Lufkin,[1,3] Bradley A. Jabour,[1] William N. Hanafee[1]

**Purpose:** To describe fat-suppression failure artifacts and to caution against their misinterpretation. **Method:** Magnetic-susceptibility artifacts were studied in a phantom model and the results were compared to MR images obtained in clinical cases. **Findings:** Artifacts manifested themselves as regions of focal fat-suppression failure and appeared as bright signals without geometric distortions at magnetic-susceptibility interfaces along the static field (z) direction. The location and extent of these artifacts were independent of either frequency or phase-encoding direction and are different from those observed in gradient-echo images. **Conclusion:** In representative clinical MR exams, these artifacts were identified in the high nasopharynx and low orbit and should not be misinterpreted as pathology.

**Index terms:** Magnetic resonance, artifacts; Magnetic resonance, fat suppression; Brain, magnetic resonance; Neck, magnetic resonance

AJNR 13:879–884, May/June 1992

Fat-suppression magnetic resonance (MR) imaging is a recently available technique that can distinguish the signal of fat from water and diminish chemical shift misregistration artifacts. This technique has been applied to several areas of the body and has been found useful for the detection and delineation of pathology. Fat-suppression techniques are particularly valuable in regions where nonfatty tissues are surrounded by fat (ie, the orbit, head and neck, and spine), since the high signal intensity of fat can often obscure adjacent pathologic processes.

A variety of fat-suppression techniques have been described, including those based on chemical shift-selective presaturation pulses (1–8), phase-difference discrimination (9–13), saturation of signals from short T1-relaxation tissue (14–16), and variation of frequency encoding gradients (17–18). Fat suppression with frequency-selective presaturation is a simple and valuable technique that requires minor modification of the standard multislice spin-echo technique, but no additional postprocessing. However, focal failure of fat suppression can occur with this technique, which results in high signal at the air/fat interfaces. The main purpose of this report is to describe this artifact so that it is not misinterpreted as pathology. In this study, both specially designed phantom and clinical studies are presented.

## Materials and Methods

All images were obtained on a 1.5-T superconducting magnet (General Electric Medical Systems, Milwaukee, WI; 4.0 Advantage). The fat-suppression technique used in this study is achieved by means of a frequency-selective presaturation pulse centered on the fat resonance followed by a homospoil gradient (6–8). The presaturation pulse converts the bulk z-magnetization of fat into xy-magnetization, whereas the water magnetization remains along the z-axis (the physical z axis is aligned parallel to the long axis of the magnet bore in our superconducting magnet). A homospoil slice-selection gradient is then applied, which dephases the xy-magnetization of fat. Thus no coherent

Received June 11, 1992; revision requested September 4; revision received on October 31 and accepted on December 6.

Presented at the 29th Annual Meeting of the ASNR, Washington DC, June 13, 1991.

[1] Department of Radiological Sciences, University of California, Los Angeles School of Medicine, Los Angeles, CA.

[2] Department of Radiology, Chiba University School of Medicine, 1-8-1 Inohana Chiba, Chiba, JAPAN 280.

[3] Address reprint requests to R. Lufkin, Department of Radiological Sciences, UCLA Medical Center, 10833 Le Conte Avenue, Los Angeles, CA 90024-1721.

AJNR 13:879–884, May/June 1992 0195-6108/92/1303-0879
© American Society of Neuroradiology

magnetization of fat remains. At this point, implementation of the usual spin-echo sequence gives only signals that originate from the water peak. The presaturation and homospoil gradient are repeated immediately before the beginning of each excitation pulse of a given repetition time (TR), insuring that no longitudinal magnetization from the saturated fat is present. The presaturation pulse and homospoil gradient precede each slice-selective pulse in the multislice sequence.

For the phantom studies, T1-weighted SE images (600/20/2 (TRmsec/TEmsec/excitations)) sequences and T2-weighted SE images (2000/80/1) were obtained with fat-suppression technique in axial, coronal, and sagittal planes. Three fields of view (FOV) (16, 20, and 30 cm) were tested. A 256 × 192 matrix size was used in conjunction with a standard head coil. The slice thickness was 5 mm, with a 1.5-mm gap.

The phantom consisted of three plastic containers of different sizes. An innermost, empty container was fixed within the middle-sized container of vegetable oil. An outermost container was filled with saline. This phantom provided air/fat and fat/water interfaces respectively (Fig. 1). The fact that the fat/water/air interfaces used in the phantom are not contiguous but are actually separated by thin layers of plastic results in a model that is not "perfect." For the purposes of this paper, we accept this limitation as not being unlike the clinical situations that we encounter.

In addition, MR scans of two patients with this artifact who were being examined for unrelated pathology are included as clinical examples.

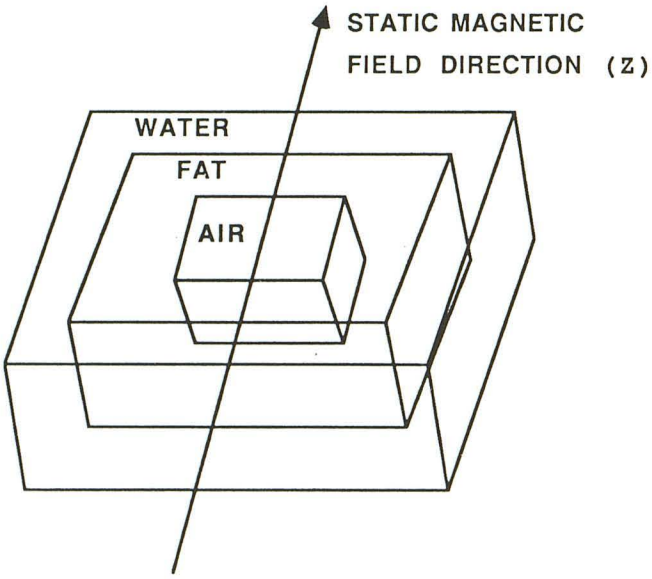


Fig. 1. Phantom used to identify susceptibility effects in frequency-selective fat-suppression image. The z axis is indicated by the *arrow*.

## Results

Phantom images showed artifacts manifested as regions of fat-suppression failure at the air/fat interfaces along the static magnetic-field direction (z-direction). This occurred regardless of the image acquisition plane. Fat signal at the air/fat interfaces along the xy-direction was completely suppressed (Fig. 2). The focal fat-suppression failure was not associated with any geometric distortions. The location and extent of this artifact were independent of either phase encoding or frequency axis.

Conventional chemical shift-misregistration errors were seen along fat/water interfaces along the frequency-encoded axis. They were independent of the fat-suppression failure artifacts (Fig. 3).

The fat-suppression failure artifacts were observed in both T1- and T2-weighted fat-suppression images to the identical extent, implying that they are independent of pulse-sequence timing considerations. The extent of the artifact was independent of gradient amplitude along xy-direction, since no significant change of the artifact was identified with varying the FOV (Fig. 4). This is in distinction to the chemical shift-misregistra-

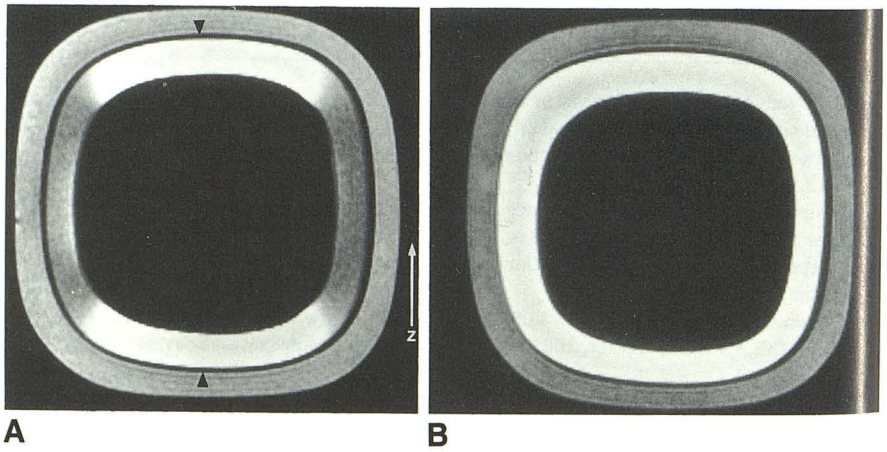


Fig. 2. Coronal images of phantom (SE 600/20); the z axis is indicated by the *arrow* (*z*).

*A*, Image with fat suppression. Fat-suppression failure is identified at air/fat interfaces along the static magnetic-field direction (*arrowheads*). However, there is no significant geometric distortion.

*B*, Image without fat suppression.

tion errors that increased as the gradient amplitude was lowered to produce larger FOVs. (Fig. 4). By repositioning the phantom such that one air/fat interface was in the center of the head coil and the other was at the edge of the coil along the z-direction, the artifact still appeared at the same location (Fig. 5). This result suggests that the artifact appearance is not related to the position of the phantom relative to the isocenter of the magnet.

On fat-suppression MR images of the skull base, artifactual high signal was observed at the junction of well-pneumatized sphenoid sinus and bone marrow of clivus (Fig. 6). However, the signal from the fat posterior to the antrum, which is not oriented along the z (craniocaudal) axis relative to the maxillary antrum, was well-suppressed. In another example of fat-suppression MR images of the orbital region, bright signal was identified in the retrobulbar space. This could be mistaken for orbital pathology (Fig. 7), but is due to the artifact at the high-susceptibility interface between air and fat. The orbital fat in this area was located above (along the z axis) the maxillary sinus. These artifacts were identified at the inferior aspect of orbital fat as well as the bone marrow of the skull base in cases with well-developed paranasal sinuses and large pharyngeal airway.

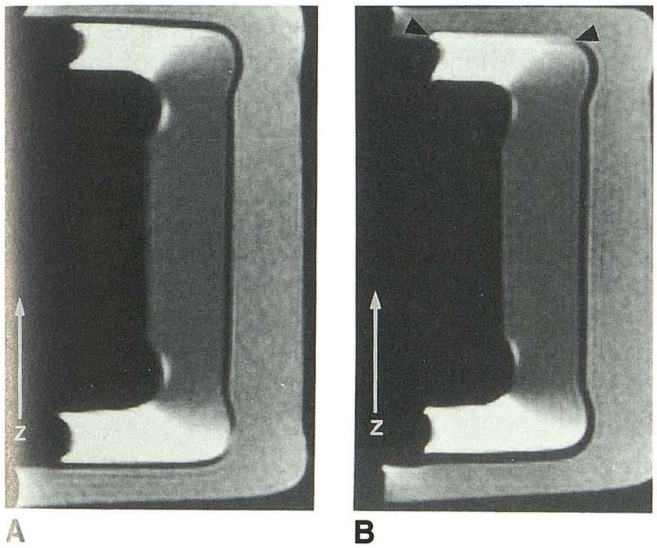


Fig. 3. Sagittal fat-suppressed image of phantom (SE 600/20). The z axis is indicated by the *arrow* (*z*). Frequency-encoding direction is set to horizontal direction in image *A*, and to vertical direction in image *B*. The location and extent of artifacts are independent of frequency-encoding direction. Chemical shift-misregistration artifact is present at fat/water interfaces in image *B* (*arrowheads*).

## Discussion

In this study, phantom and clinical MR images demonstrated potentially confusing focal fat-suppression failure along the static magnetic-field direction where there are large differences in magnetic susceptibility between adjacent regions. This artifact was most troublesome in areas of the nasopharynx and orbits because of their craniocaudal (static magnetic-field direction) orientation in superconducting magnets relative to the paranasal sinuses and nasopharynx. These focal fat-suppression failures are confusing and could simulate pathology in these regions. Our results are largely observational and this paper does not purport to develop a definitive basic understanding of the mechanisms of this artifact.

We hypothesize that this artifact arises from resonant-frequency shifts due to focal magnetic-field inhomogeneity at the air/tissue interfaces, which result in partial local failure of the presaturation pulse. Magnetic-field homogeneity is distorted where adjacent tissues differ greatly in magnetic susceptibility, because spatial variations in magnetic susceptibility produce intrinsic magnetic gradients in these regions. The majority of tissues in the body have a slightly negative sus-

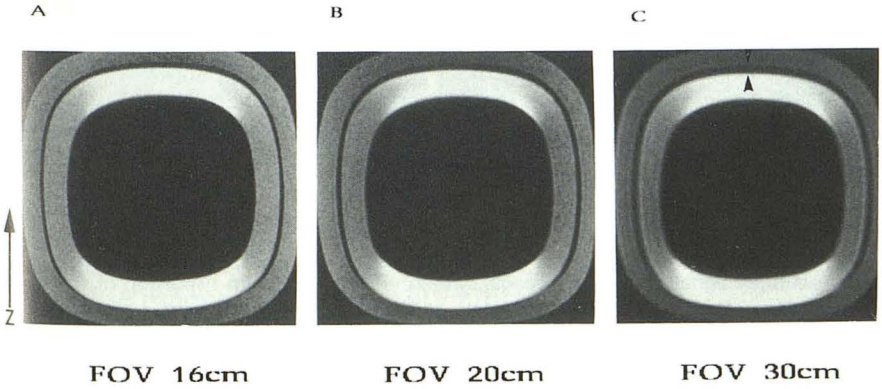


Fig. 4. Coronal fat-suppressed images of phantom with different size of FOVs. The z axis is indicated by the *arrow* (*z*). No significant change is identified with varying the size of FOVs. Note the chemical shift-misregistration artifacts along the superior fat/water interface due to decreasing gradient amplitude (*arrowheads*). *A*, 16 cm; *B*, 20 cm; *C*, 30 cm.

ceptibility and are called diamagnetic (weaken the applied magnetic field). However air has only about 1/1000 the susceptibility of most solids (19). This large difference results in air representing the equivalent of a source of negative magnetization compared with tissue. Therefore, focal magnetic-field inhomogeneity can occur due to intrinsic field gradients across the imaging voxel.

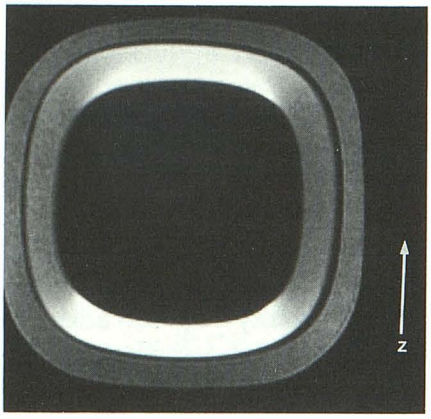


Fig. 5. Fat-suppressed image after repositioning one air/fat interface to be located in the center of the field and the other to be at the edge of the field. The artifacts still appear even if the air/fat interface is placed in the center of the field. Thus, the appearance of the artifacts appears to be independent of position relative to the isocenter of the magnet. A water bag is placed above the phantom. The z axis is indicated by the *arrow* (*z*).

The intrinsic gradient causes shift of the actual resonant frequency of the protons in fat and results in the failure of frequency-selective presaturation pulses. The reason that this artifact was only observed along the static magnetic-field direction is not entirely understood, but may be related to the fact that the static magnetic field of the system is usually two to three orders of magnitude greater than magnetic-field gradients.

The fat-suppression failure artifact that we are describing is different from other forms of magnetic susceptibility artifacts that occur along the frequency-encoded or readout axis. The so called "magnetic-susceptibility artifact" is characterized by geometric distortion of the object along the frequency-encoding axis and signal loss due to rapid-spin dephasing caused by focal magnetic-field inhomogeneity (20–22). This is more pronounced in gradient recalled-echo images than in spin-echo images because of the lack of the 180° refocusing pulse in the former techniques. The artifacts observed in frequency-selective fat-suppression images were due to resonant-frequency shifts caused by focal magnetic-field inhomogeneity. Focal fat-suppression failure showed no significant change with switching phase- and frequency-encoding axis nor with varying the gradient amplitude. The characteristics of this artifact are different from so-called magnetic-susceptibility artifacts (Table 1). How-

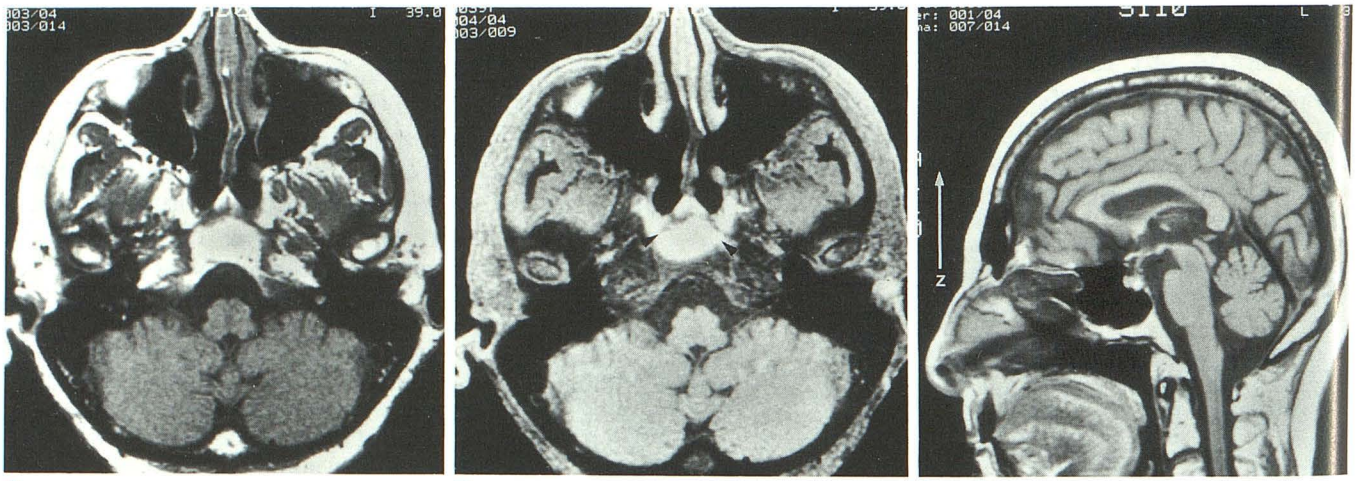


Fig. 6. Clinical example of fat-suppression failure in the clivus.

*A*, Conventional axial T1-weighted image of skull base.

*B*, Fat-suppressed axial T1-weighted image shows a high signal area (*arrowheads*), which corresponds with a portion of the fatty marrow of clivus overlying the airway.

*C*, T1-weighted sagittal image shows that the portion of the clivus that showed high signal is located between a well-pneumatized sphenoid sinus and the airway. The z axis is indicated by the *arrow* (*z*).

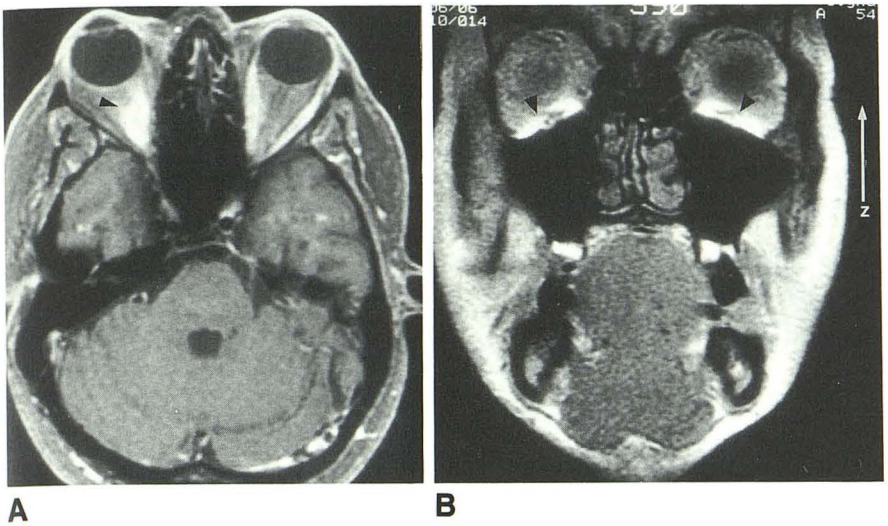


Fig. 7. Example of fat-suppression failure in the orbits.

*A*, Axial T1-weighted fat-suppression image shows high signal area in the retrobulbar space (*arrowhead*), which is simulating orbital pathology. This is artifact at susceptibility interfaces between lower part of orbital fat and upper portion of maxillary sinus.

*B*, Coronal image in the same patient also showing high signal (*arrowheads*) which is not due to the inferior rectus muscles. The z axis is indicated by the *arrow* (*z*).

**TABLE 1: Characteristics of magnetic-susceptibility artifacts and fat-suppression failure**

| Characteristics | Magnetic-Susceptibility Artifacts | Fat-Suppression Failure |
|---|---|---|
| Axis involved | Frequency-encoding direction | Static magnetic-field direction (z axis for superconducting magnets) |
| Appearance | Signal loss with geometric distortion | Focal high signal without geometric distortion |
| Mechanism | Rapid-spin dephasing, spatial misregistration | Resonant frequency shift causing failure of fat presaturation |
| Location | Magnetic-susceptibility interfaces | Magnetic-susceptibility interfaces |

ever, both artifacts are the result of focal magnetic-field inhomogeneity at bulk susceptibility interfaces.

Fat-suppression failure has also been seen in areas of changing tissue geometry such as the submental or submandibular regions with frequency-selective presaturation technique. These artifacts also occur in the craniocaudal (along the static magnetic field) direction. Fat-suppression failure observed in subcutaneous fat may be of little problem in clinical diagnosis. However, these artifacts did occur in areas of constant imaging volume such as the nasopharynx and orbits because of their craniocaudal orientation relative to the paranasal sinuses. Therefore, these regions were most troublesome and could present difficulties in clinical diagnosis. Although the benefit of contrast-enhanced fat-suppression imaging has been reported in the head and neck region (23), these magnetic-susceptibility artifacts could be clinically confusing without the availability of precontrast fat-suppression images for comparison. It should be remembered that all bright lesions on enhanced scans are not necessarily associated with pathologic process. The understanding of the geometric relationship between air and high signal regions in frequency-selective fat-suppression technique is extremely important to prevent misdiagnosis.

## Acknowledgments

The authors would like to thank Bobby Keen, Keyvan Farahani, and Julien Keesing for their generous assistance in this project.

## References

1. Maudsley AA, Hilal SK, Perman WH, Simon HE. Spatially resolved high resolution spectroscopy by four dimensional NMR. *J Magn Reson* 1983;51:147–153
2. Bottomley PA, Foster TH, Leue WM. Chemical imaging of the brain by NMR. *Lancet* 1984;1:1120–1123
3. Hasse A, Frahm J, Hanicke W, Matthaei, D. 1H NMR chemical shift selective (CHESS) imaging. *Phys Med Biol* 1985;4:341–344

4. Dumoulin CL. The application of multiple-quantum technique for the suppression of water signals in 1H NMR spectra. *J Magn Reson* 1985; 64:38–46
5. Axel L, Dougherty L. Chemical shift selective magnetic resonance imaging of multiple line spectra by selective saturation. *J Magn Reson* 1985;66:189–194
6. Keller PJ, Hunter WW, Schmalbrock P. Multisection fat-water imaging with chemical shift selective presaturation. *Radiology* 1987;164: 539–541
7. Frahm J, Hasse A, Hanicke W, Matthaei D, Bomsdorf H, Helzel T. Chemical shift selective MR imaging using a whole body magnet. *Radiology* 1985;156:441–444
8. Rosen BR, Wedeen VJ, Brady TJ. Selective saturation NMR imaging. *J Comput Assist Tomogr* 1984;8:813–818
9. Dixon WT. Simple proton spectroscopic imaging. *Radiology* 1984; 153:189–194
10. Kunz D. Double pulse echoes: a novel approach for fat-water separation in magnetic resonance imaging. *Magn Reson Med* 1986;3: 639–643
11. Szumowski J, Plewes DB. Separation of lipid and water MR imaging signals by Chopper averaging in the time domain. *Radiology* 1987; 165:246–250
12. Yeung HN, Kormos DW. Separation of true fat and water images by correcting magnetic field inhomogeneity in situ. *Radiology* 1986; 159:783–786
13. Szumowski J, Eisen JK, Vintski S, Haake PW, Plewes DB. Hybrid methods of chemical shift imaging. *Magn Reson Med* 1989;9: 379–388
14. Bydder GM, Young IR. MR imaging: clinical use of the inversion recovery sequence. *J Comput Assist Tomogr* 1985;9:659–675
15. Dwyer AJ, Frank JA, Sank VJ, Reinig JW, Hickey AM, Doppman JL. Short TI inversion-recovery pulse sequence: analysis and clinical experience in cancer imaging. *Radiology* 1988;168:827–836
16. Atlas SW, Grossman RI, Hackey DB, Goldberg HI, Bilaniuk LT, Zimmerman RA. STIR imaging of the orbit. *AJR* 1988;151: 1025–1030
17. Axel L, Glover G, Pelc N. Chemical shift magnetic resonance imaging of two-line spectra by gradient reversal. *Magn Reson Med* 1985;2: 428–436
18. Twieg DR, McKinnon GC. Multiple output chemical shift imaging (MOCSI): a rapid method for chemical shift imaging and localized moderate resolution NMR spectroscopy. *Magn Reson Imaging* 1986; 4:118
19. Joseph PM, Atlas SW. Artifacts: magnetic resonance imaging of the brain and spine. Atlas SW, ed. New York: Raven, 1991:109–113
20. Ludeke KM, Roschmann P, Tichler R. Susceptibility artifacts in NMR imaging. *Magn Reson Imaging* 1985;3:329–343
21. Czervionke LF, Daniels DL, Wehrli FW, et al. Magnetic susceptibility artifacts in gradient-recalled echo MR imaging. *AJNR* 1988;9: 1149–1155
22. Schick RM, Wismer GL, Davis KR. Magnetic susceptibility effects secondary to out-of-plane air in fast MR scanning *AJNR* 1988;9: 439–442
23. Barkos JA, Dillon WP, Chew WM. Orbit, skull base, and pharynx: contrast enhanced fat suppression MR imaging. *Radiology* 1991; 179:191–198